

Efficient and Controllable Vapor to Solid doping of the Polythiophene P3HT by Low Temperature Vapor Phase Infiltration

Weike Wang,^{a,b,c} Chaoqiu Chen,^a Christopher Tollan,^b Fan Yang,^b Yong Qin^{a*} and Mato Knez^{b,d*}

^aState Key Laboratory of Coal Conversion, Institute of Coal Chemistry, Chinese Academy of Sciences, Taiyuan, 030001, China.

^bCIC nanoGUNE, Tolosa Hiribidea, 76, 20018 Donostia-San Sebastian, Spain.

^cUniversity of Chinese Academy of Sciences, Beijing, 100049, China.

^dIKERBASQUE, Basque Foundation for Science, 48011 Bilbao, Spain.

E-mail: qinyong@sxicc.ac.cn, E-mail: m.knez@nanogune.eu

Keyword: vapor phase infiltration, ALD, doping, poly(3-hexyl)thiophene, stability

Abstract

Efficient doping of organic semiconductors is an important prerequisite for the fabrication of high performance organic electronic devices. In this work, we describe a novel single precursor low-temperature (70 °C) vapor phase infiltration (VPI) process to dope poly(3-hexyl)thiophene

(P3HT). The infiltration is performed with the metal containing atomic layer deposition (ALD) precursor MoCl_5 . The conductivities of the polymer are assessed with four-point probe measurements and showed significant enhancement by up to 5 orders of magnitude, confirming the efficiency of the VPI process. The chemical changes resulting from the infiltration of P3HT are characterized applying UV-Vis-NIR, Raman spectroscopy, and FTIR. The crystalline state of the material is analyzed by X-ray diffraction (XRD). SEM micrographs and AFM images show that the morphologies of the samples before and after MoCl_5 infiltration process do not seriously change. TEM images of cross-sections of the thin film clearly show that the vapor phase infiltration process results in the incorporation of Mo into the bulk of the polymer.

Introduction

Over the past years, organic semiconductors (OSCs) have been extensively investigated due to their tremendous importance as integral part of a wide range of electrical devices.¹⁻⁴ For instance, previous studies have reported on enhanced mobilities of charge carriers in field-effect transistors (FETs) achieved by trap filling,⁵ improved charge injection in light-emitting diodes (LEDs)^{6,7} and, more recently, superior power conversion efficiencies in organic photovoltaics.⁸⁻¹³ The development of inorganic semiconductor devices has revealed that crucially important steps for enabling engineering of efficient electronics include controllable doping and realization of stable and controllable doped transport layers for both p- and n- type materials. The same considerations apply for the organic counterpart as well. However, doping strategies for OSCs are typically dissimilar to those for their inorganic counterparts and thus optimal schemes need to be evaluated from scratch. Even though doped OSC thin films have been shown to exhibit

conductivities to 5-8 orders of magnitude higher than undoped films,^{14,15} better understanding of the chemistry that occurs upon doping and evaluation of various strategies for improving the efficiency is expected to result in even more efficient OSCs, which will strongly impact the emerging field of organic electronics.

Doping of inorganic semiconductors is meanwhile well developed. Controlled introduction of atomic or ionic impurities into semiconductors became the fundamental enabler for the functionality of modern electronic devices as we experience them nowadays.¹⁶ The doping process allows tuning the band alignment at interfaces and markedly increases the conductivity even at ultralow doping ratios, as typically every covalently bound dopant atom donates one mobile charge carrier to the highly crystalline and ultra-pure semiconductor matrix. In contrast, doping of OSCs is achieved by adding comparatively strong electron acceptors or donors, resulting in a significant increase of the charge carrier density and therefore conductivity of such materials. Stable p-type doping is nowadays typically achieved by introducing transition metal oxides such as MoO₃¹⁷ or WO₃¹⁸ into the polymer, or by adding molecular π -electron acceptors, for example, tetracyano-2,3,5,6-tetrafluoroquinodimethane (F4TCNQ),¹⁹⁻²¹ 2,2'-bis(trifluoromethyl)-9,9'-diphenylfluorene (F6TCNNQ),²² or 1,4,5,8,9,11-hexaazatriphenylenehexacarbonitrile(HATCN).²³ The principle of doping with molecular π -electron acceptors has been proven to be applicable to a wide range of molecular semiconductors and polymers. The resulting conductivity of such F4TCNQ-doped organic materials can exceed 1 S/cm at highest dopant concentrations.²⁴ Among the various molecular dopants, F4TCNQ gained prominence as reference dopant. The fundamental mechanisms that determine the concentration and mobility of mobile holes in F4TCNQ-doped samples of the polymer poly(3-hexyl)thiophene, P3HT, have been identified and showed that in this particular donor-acceptor

couple almost all employed F4TCNQ molecules undergo integer charge transfer (ICT), meaning that an electron is fully transferred from the π -electron system of a P3HT site to the F4TCNQ acceptor. This eventually results in positively charged P3HT (P3HT^+) and negatively charged F4TCNQ (F4TCNQ^-).²⁵ Thus, F4TCNQ-doping leads to a strong increase in the density of mobile charge carriers and consequently the electrical conductivity. However, as an alternative to the common π -electron acceptors, some recent reports introduced the possibility of doping of polymers with Lewis acids. The Bazan and Neher groups have studied the optical and charge carrier transport properties of various polymers which were doped by the strong Lewis acid tris(pentafluorophenyl)-borane (BCF).²⁵⁻²⁹ The effect has been explained with a formation of Lewis acid-base adducts. In the case of p-type doping with BFC, the electrophilic borane center binds to a moiety carrying an accessible lone pair of electrons, for example, the nitrogen atoms present in pyridine or the benzothiadiazole units of the semiconductor. The binding induces a redistribution of the electron density, that is, a charge transfer between the semiconductor and dopant occurs. This will eventually change the oxidation state of each of the partners, liberating charge carriers that become available electrical conduction.

Given the already published results, the mentioned doping with Lewis acid appears to be a promising approach for obtaining efficient OSCs, but the doping process itself may still be further improved. Here, we apply a novel procedure for doping P3HT with the Lewis acid molybdenum (V) chloride (MoCl_5) and a detailed analysis of the resulting doped polymer. Doping of polymers is typically performed in liquid state, which introduces various chemical species such as solvents or byproducts of chemical reactions into the substrate with all the related potentially negative consequences for the conductivity and/or stability of the resulting material.

Besides, the possibility of shaping the polymer after doping process is often hampered because

of dopant-induced crystallization or hardening of the polymer. For avoiding such negative influences, we apply an alternative approach, vapor phase infiltration (VPI) process, for injecting the Lewis acid into the polymeric substrate. The VPI process is derived from atomic layer deposition (ALD),³⁰ and applies the same processing technology, that is, exposure of the substrates to vaporized chemicals in a pulsed manner with stringent control of the dosing parameters. This procedure allows taking advantage of the mobility of a vaporized chemical and its ability to diffuse into and react with polymeric substrates.³¹ Incorporation of inorganic materials into polymers often enhances some physical properties of the resulting composite or hybrid material.³¹⁻³⁸ For example, our earlier works demonstrated that infiltration of metal oxides or metal ions into various (bio)polymers, including spider silk,³⁶ avian egg collagen³⁷ and cellulose³⁸ by means of ALD-derived strategies often results in hybrid materials with exceptional mechanical properties. The present work shows that a similar infiltration process can also be used for doping P3HT and furthermore allows for controlling the level of conductivity of the polymer through the number of infiltration cycles applied. In conjunction with MoCl₅, P3HT acts as a Lewis base for its lone electron pairs present at the sulfur atoms of the thiophene rings. A hypothesized interaction scheme between MoCl₅ and a P3HT segment is sketched in **Figure 1**. In this manuscript we show that the introduction of MoCl₅ into P3HT by VPI leads to p-type doping via ICT, and the conductivity of P3HT/MoCl₅ can reach exceptional values of 3.01 S/cm which is up to 5 orders of magnitude higher than that of the native P3HT, while maintaining its stability for at least 30 days at ambient conditions.

Experimental Section

Film Preparation

1,2-Dichlorobenzene (DCB) was purchased from Aldrich and used as received. Poly(3-hexylthiophene-2,5-diyl) (P3HT, $M_w = 50\,000\text{ g mol}^{-1}$, 95% regioregularity) was purchased from Reike Metals, Inc. U.S.A and used as-received. As substrates, the electrically insulating glass slides were used, which were cleaned thoroughly by sonication in acetone, methanol and isopropanol for 1 h prior to coating with P3HT. For pristine films, 37 mg P3HT was dissolved in 1 mL DCB. The thin films ($\approx 35\text{ }\mu\text{m}$) were prepared via drop casting the solution on glass substrates (1.3 cm \times 1.3 cm) at ambient conditions. All samples were soft-baked at 70 °C overnight to remove excess solvent. The thicknesses of the films were measured with cross-sectional scanning electron microscopy (FEI, Quanta 250 FEG).

Vapor-phase Infiltration Process

Vapor-phase infiltration was performed using a homemade atomic layer deposition tool. Pristine P3HT films coated on glass substrates were exposed to vapors of MoCl_5 in a pulse-exposure-purge sequence with various numbers of repetition cycles. One cycle of the process consisted of following settings: the precursor (MoCl_5 , 95%, Aldrich) was pulsed into the reaction chamber for 5 s and thereafter exposure of the substrates to the vapors in the reaction chamber was allowed for 120 s. The exposure was followed by a 60 s purge step. The cycle was repeated with the number of cycles varying between 10 and 300. As carrier and purging gas N_2 (99.99%) was used. The chamber temperature was kept constant at 70 °C during the infiltration process with the base pressure of the reactor being maintained at 50 mTorr. Since at room temperature MoCl_5 is solid, heating of the precursor to 70 °C was required to obtain reasonable vapor pressure.

Characterization

Absorption spectra of the samples were recorded between 360-890 nm using a UV-Vis spectrophotometer (V-630 BIO, JASCO).

Raman spectra with a 532 nm (100× objective) exciting wavelength were collected with a Raman microscope (Alpha 300S, WITec). The laser power was kept at 0.02 mW and the acquisition time was 10-20 s for each measurement in order to avoid sample degradation. The Raman spectra were background corrected and obtained by averaging spectra obtained from five different regions of each sample.

X-ray diffraction (XRD) analysis was carried with a powder diffractometer (X'pert, PANalytical with 45 kV, 40 mA) with Ni-filtered Cu K α radiation.

Infrared spectra of the samples were recorded between 760 and 1610 cm⁻¹ with a FTIR Spectrometer (PerkinElmer, Frontier).

The morphology of the samples was characterized by scanning electron microscopy (FEI, Quanta 250 FEG) and the chemical composition was analyzed with energy-dispersive X-ray spectroscopy (EDX).

AFM analysis was performed on the P3HT-coated glass slides, employing a 5500 AFM (Keysight, Santa Clara). The AFM probe was a HQ-NSC 14/Al BS tip with an approximate radius of 8 nm. The spring constant of the cantilevers was 5 N/m and a resonance frequency of 160 KHz was used in tapping mode; data processing was done using the software Gwyddion.

TEM images and EDS analysis was carried out with an FEI Titan microscope using 300 kV in STEM mode and an EDAX SDD detector. The FIB used for lamellae preparation was a dual beam Helios Nanolab 450S from FEI. Ultramicrotome cuts for TEM analysis were done using a

Leica UC6 ultramicrotome with a Diatome ultra sonic diamond knife. The instrument was set to take 80 nm cuts. And the FIB lamellae were prepared from a glass wafer with the P3HT thin film deposited on it and after the entire wafer had undergone MoCl₅ vapor phase infiltration treatment. The block was extracted by standard methods using a Pt electron beam deposition to initially protect the sample surface before any ion beam deposition was carried out. The block was thinned to transparency on a copper "Omniprobe" grid using a 5 kV gallium ion beam at 8 pA for final surface preparation.

The conductivities of the thin films were measured applying a four-point probe technique with a source measurement unit (Keithley 2611). For each VPI experiment 4 or 5 individual samples were tested for each VPI process cycle number. The resulting conductivity, σ , was calculated according to the formula,

$$\sigma = \ln 2(I / \pi dV) \quad (1)$$

where I is the current, V is the voltage and the d is the whole polymer film thickness.

Results and Discussion

Assessment of the electrical conductivity

The functionalization of P3HT thin films with MoCl₅ through the vapor phase infiltration process resulted in the introduction of mobile carriers into the conjugated polymer, and therefore in an enhanced conductivity. In contrast to a typical ALD process or previously described ALD-based infiltration strategies, where a substrate is sequentially exposed to vapors of two precursors, here we expose the substrate to the vapor of only one precursor and allow sufficient time for the precursor to diffuse into subsurface areas of the substrate. After infiltration, we measured the

electrical characteristics of the samples. **Figure 2a** shows the room temperature I - V plots of the various fabricated P3HT samples in comparison to the untreated polymer. The thicknesses of all samples were comparable ($\approx 35 \mu\text{m}$). The plots of P3HT/MoCl₅ are linear, confirming ohmic behavior over the whole measurement range. Untreated P3HT thin films act as reference with conductivity values of 1.44×10^{-5} S/cm. The increase in conductivity confirms the possibility of using the vaporized Lewis acid MoCl₅ for doping P3HT. The values for the electrical conductivities of the samples were extracted from the slopes of the I - V plots. An important observation resulting from the measurements is that the conductivity of the doped P3HT films stands in non-linear correlation with the number of infiltration cycles as can be seen in **Figure 2b**. The peak value of the conductivity with 3.01 S/cm is reached after 100 infiltration cycles, while lower and higher number of cycles result in lower conductivities.

UV-Vis spectroscopy

Successful p-doping of the conjugated polymer P3HT by the Lewis acid MoCl₅ through applying the VPI process was further confirmed by various spectroscopies. Optical (absorption and emission) as well as Raman and Fourier Transform Infrared (FTIR) spectra were taken from the infiltrated samples to confirm and identify chemical changes in the polymer.

The UV-Vis spectra of P3HT and P3HT/MoCl₅ after application of various VPI cycle numbers are shown in **Figure 3a**. Pristine P3HT strongly absorbs in the region between 500 and 650 nm, with three distinct maxima at 518, 552, and 605 nm. These three bands are typically attributed to the ordered lamellar phase of P3HT and correlate to electronic π - π^* transitions.^{39,40} The band at 552 nm is attributed to the absorption of extended conjugated systems and the band at 605 nm is attributed to interchain interactions. The UV-Vis absorption spectra acquired from P3HT/MoCl₅ (10cycles) largely correspond to those of pristine P3HT, albeit with a lower intensity.

Interestingly, with an increasing number of VPI cycles, and thus doping concentration, a bleaching of the main π - π^* absorption band of P3HT centered at ≈ 530 nm was observed. At the same time a new absorption maximum at 478 nm developed, accompanied by a gradual increase in the sub-gap absorption in the infrared region around 826 nm (**Figure 3a**).^{39,40} The reduction of the main π - π^* absorption band suggests that the presence of MoCl₅ in elevated concentration (100 VPI cycles) weakens the interchain interactions, resulting from a disordering effect of MoCl₅ on the crystalline phase of P3HT. These observations point towards the presence of a ground-state charge transfer from P3HT to MoCl₅, triggered by an effective transfer of electrons from the polymer (*viz.* oxidation) to the electron-poor MoCl₅. This eventually results in the formation of positive polarons. It is worth noting that the P3HT/MoCl₅ samples are temporally very stable. This becomes obvious if the stability of our infiltrated samples is compared to that of reported P3HT/FTS. In the latter case, upon exposure to air, the absorption spectra, the original color, and the initial high electrical resistivity recover within 4-5 days in the dark or within hours under illumination,⁴¹ while in the present case the absorption spectra of MoCl₅-doped P3HT (**Figure 3b**), the perceived color, and the measured conductivities only marginally changed upon exposure of the samples to air in ambient conditions for 30 days.

Raman spectroscopy

Figure 4 shows a typical Raman spectrum of a P3HT thin film excited with a laser operating at 532 nm. Various Raman modes can be observed in the region 700-1545 cm⁻¹: the main in-plane ring skeleton modes at 1452 cm⁻¹ (symmetric C=C stretching) and at 1384 cm⁻¹ (C-C intra-ring stretching), the inter-ring C-C stretching mode at 1212 cm⁻¹, the C-H bending mode with C-C inter-ring stretching mode at 1185 cm⁻¹, and the C-S-C deformation mode at 731 cm⁻¹.⁴² Among the observed Raman modes, we will focus on the two main in-plane ring skeleton modes at 1452

and 1384 cm^{-1} , and the C-S-C deformation mode at 731 cm^{-1} , as those are expected to be sensitive to electron delocalization and thus the extension of the conjugation in P3HT.

From the spectra in **Figure 4** and the respective data in **Table 1**, one can observe that the Raman peak of the P3HT C=C mode shifts from 1452 cm^{-1} to 1457 cm^{-1} after infiltration. This C=C peak position and its width are indicative of the degree of molecular order in P3HT.⁴² The position shift of ca. 5 cm^{-1} together with the increasing full width at half maximum (fwhm) from 30 cm^{-1} to 47 cm^{-1} after infiltration indicate a disturbance of the order in the P3HT upon infiltration. Further significant changes can be observed in the peak position and fwhm of the C-C mode. The peak shifts by 4 cm^{-1} with the fwhm rising from 11 cm^{-1} to 22 cm^{-1} . Similar to the case of C=C mode described above, this change in the C-C mode also indicates a disturbance of the molecular order in P3HT after MoCl₅ VPI process. In addition, we also note significant changes in the peak position and fwhm of the C-S-C mode, namely a slight shift from 731 cm^{-1} to 728 cm^{-1} with the fwhm rising from 9 cm^{-1} to 26 cm^{-1} . This is an obvious sign for ring deformations in the P3HT molecule, which most likely result from a strong interaction between Mo atoms and S atoms after the VPI process, which is confirmed by the XPS spectra of S 2p peak in Figure S1 (Supporting Information). The peak located at binding energy of 164.56 eV corresponds to S 2p line of pristine P3HT. While after 5 cycles MoCl₅ infiltration process, the intensity of S 2p of the pristine P3HT decreases, and a new peak located at binding energy of 163.39 eV developed, which might be due to the S interacting with Mo, indicating the electronic exchange between P3HT and MoCl₅. Considering the above-mentioned, we conclude that the MoCl₅ VPI process has significantly decreased the degree of order of P3HT molecules in the resulting P3HT/MoCl₅ thin film. Furthermore, the changes in the peak position and fwhm of both the C-C mode and the C-S-C mode strongly suggest the formation of positive polarons in the polymer matrix.

Infrared spectra

More details about the occurring chemical changes in the polymer after infiltration can be extracted from the infrared spectra of P3HT before and after infiltration, which are shown in **Figure 5**. The black spectrum is taken from the untreated P3HT and is used as reference for identifying chemical changes. The red and blue spectra were measured from P3HT/MoCl₅ samples after processing with 10 and 30 infiltration cycles, respectively. The latter spectra indicate that the main carriers that were generated were positive polarons, which can be derived from the observation of the polaron bands at 1391, 1282, 1143, 1078, 979, and 868 cm⁻¹, respectively, after the 30 cycles MoCl₅ VPI process.⁴³ Especially the bands observed at 1391 and 1392 cm⁻¹, respectively, evolve newly after the MoCl₅ VPI process. Furthermore, the shifts of modes that were observed upon applying different VPI cycle numbers in **Figure 5** are changes in modes that originate from effective conjugation within the molecules.

X-ray diffraction

In order to investigate the internal structure of the P3HT thin film, X-ray diffraction (XRD) was applied. **Figure 6** shows XRD patterns of untreated P3HT and P3HT/MoCl₅ after various infiltration cycle numbers (30, 50 and 100). The untreated P3HT shows a (100) reflection peak, which is due to the lamellar layered structure.¹⁹ The further (100), (200), and (300) diffraction peaks indicate crystallinity with edge-on chain orientation.¹³ The out-of-plane reflection peak (010) results from π - π interchain stacking.⁴⁴ With an increasing number of MoCl₅ VPI cycles, the (*n*00) diffraction peaks shifted towards lower angles, which confirms structural perturbations in the alkyl stacking direction,⁴⁵ a sign that the lamellar spacing increases. The (010) diffraction peak shifted to larger angles, which can be explained with the in-plane π -stacking spacing decreasing, thereby indicating less ordering in the doped film after the MoCl₅ VPI process. A

significant increase in peak width in the ($n00$) signals further confirms that the infiltrated MoCl_5 significantly increases the disorder in the alkyl stacking direction. The MoCl_5 VPI process significantly affects the order and d-spacing in the alkyl stacking direction, which will influence the electrical properties of P3HT thin film.⁴⁶ This is confirmed by the present study.

SEM, AFM and TEM

Scanning electron microscopy (SEM, **Figure 7**) and atomic force microscopy (AFM, **Figure 8**) were applied to evaluate the morphology of the samples before and after VPI process. These images show that after infiltration with MoCl_5 , the P3HT surface becomes decorated with nanoscale islands. Based on the AFM images, the surface roughness increases from 18.4 nm to 22.1 nm. A possible reason for that may be the aforementioned intercalation of MoCl_5 into the polymeric matrix, which results in swelling of the polymer. Consequently, release of the stress may occur on a local level by expulsion of polymeric material to the surface. With an elevated Mo-precursor concentration at the surface of the polymer and strong electrostatic interactions between the negatively charged MoCl_5^- and the positively charged, P3HT^+ , we can expect some local aggregation of the crystalline P3HT to nanoscale islands. These islands or roughnesses would expectedly have a negative surface dipole moment and thus repel each other, which may explain the high dispersion and uniform size distribution observed in the SEM and AFM images.⁴⁷ In **Figure 9**, such elevated concentration of Mo at the surface of the polymer can be seen. The TEM-EDX images show cross-sectioned area of untreated P3HT and MoCl_5 -infiltrated P3HT (100cycles, 70 °C), prepared by a focused ion beam. Besides the higher concentration at the surface, a considerable amount of Mo is found in the bulk of the sample, which clearly shows that the vapor phase infiltration process results in the incorporation of Mo-precursor into the bulk of the polymer. Aggregations are found in the bulk of the samples, which indicate a similar type

of crystallite formation in the bulk as observed on the surface of the polymer. Being spatially isolated, those aggregates, however, are not considered to be the main reason for the increase in conductivity, but rather the well dispersed Mo-precursor in the polymer matrix.

Conclusions

To summarize, we have demonstrated a novel and efficient way of doping P3HT by applying an ALD-derived single precursor low temperature vapor phase infiltration (VPI) process. As a result, a great increase of the electrical conductivity of P3HT was observed. Upon doping by infiltration with Lewis acid MoCl₅, the conductivity rose by up to 5 orders of magnitude, reaching 3.01 S/cm at its best. More importantly, the P3HT/MoCl₅ thin films exhibited exceptional stability in ambient conditions, largely outperforming the stability of previously reported P3HT/FTS. Doping with MoCl₅ from the vapor phase results in a local oxidation of the P3HT, owing to the Lewis basic character that P3HT shows in conjunction with MoCl₅. The lone electron pairs at the sulfur atoms of the thiophene rings in P3HT can donate negative charge to the MoCl₅ with themselves becoming rather positively charged. The results are not only significant for the novel process to dope P3HT and obtain better stability of the doped polymer at ambient conditions, but also for the possibility to perform top-down doping of already pre-manufactured P3HT, which allows for better shaping of the material and therefore more efficient device fabrication. The results encourage future work, particularly the adaptation of similar infiltration processes to more challenging conductive polymers, other p-type molecular crystals, including rubrene and tereacene, or further n-type molecular crystals.

AUTHOR INFORMATION

Corresponding Author

*Yong Qin. E-mail: qinyong@sxicc.ac.cn

*Mato Knez. E-mail: m.knez@nanogune.eu

Author Contributions

The manuscript was written through contributions of all authors. All authors have given approval to the final version of the manuscript.

Notes

The authors declare no competing financial interest.

ACKNOWLEDGMENT

We appreciate the Hundred Talent Program of the Chinese Academy of Sciences, Youth Innovation Promotion Association of the Chinese Academy of Sciences, the Hundred Talent Program of ShanXi Province. The authors are grateful for funding from European Union FP7 Programme under grant agreement numbers 607232 (Marie Curie-ITN THINFACE) and 322158 (Marie Curie-CIG ARTEN), and the Spanish Ministry of Economy and Competitiveness (MINECO) within grant agreement no. MAT2016-77393-R. The authors thank Dr. Aitziber Eleta for her support in AFM microscopy, and Dr. Andrey Chuvilin for his support in the TEM characterization. The work was performed with the PCAM European doctorate.

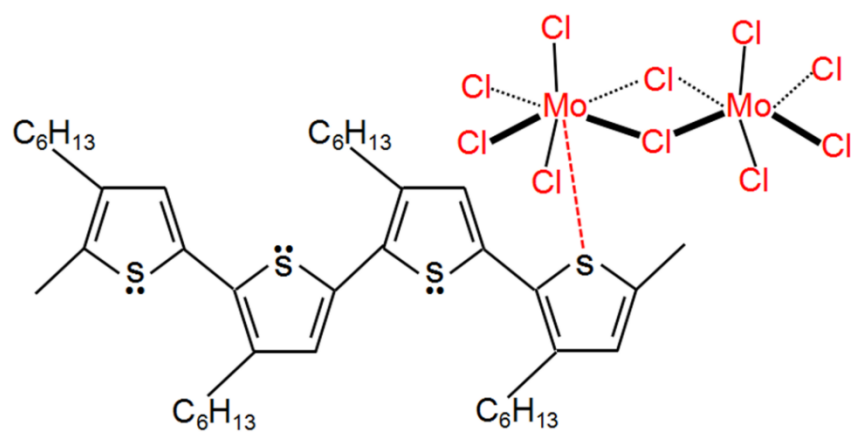


Figure 1. Schematic of the proposed Lewis acid-base adduct formation between poly(3-hexylthiophene), P3HT, and molybdenum(V)chloride, MoCl₅.

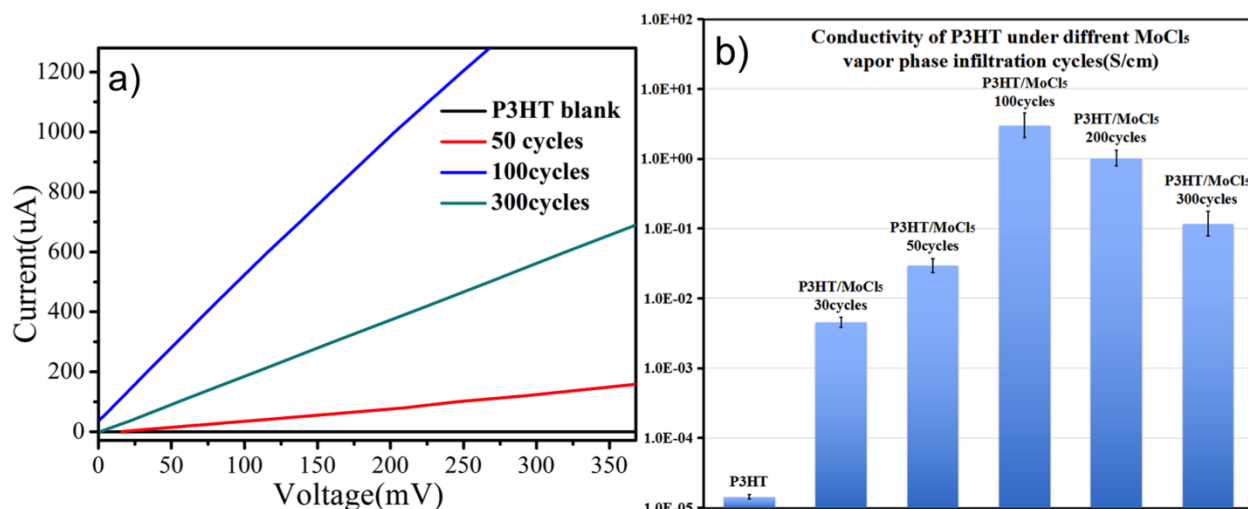


Figure 2. a) I - V plots of undoped P3HT (black) and MoCl_5 -doped P3HT after 50 (red), 100 (blue), and 300 (cyan) processing cycles; b) comparison of the conductivities of undoped P3HT blank and P3HT doped with MoCl_5 after various cycles numbers (30, 50, 100, 200, and 300 cycles) processed at 70°C .

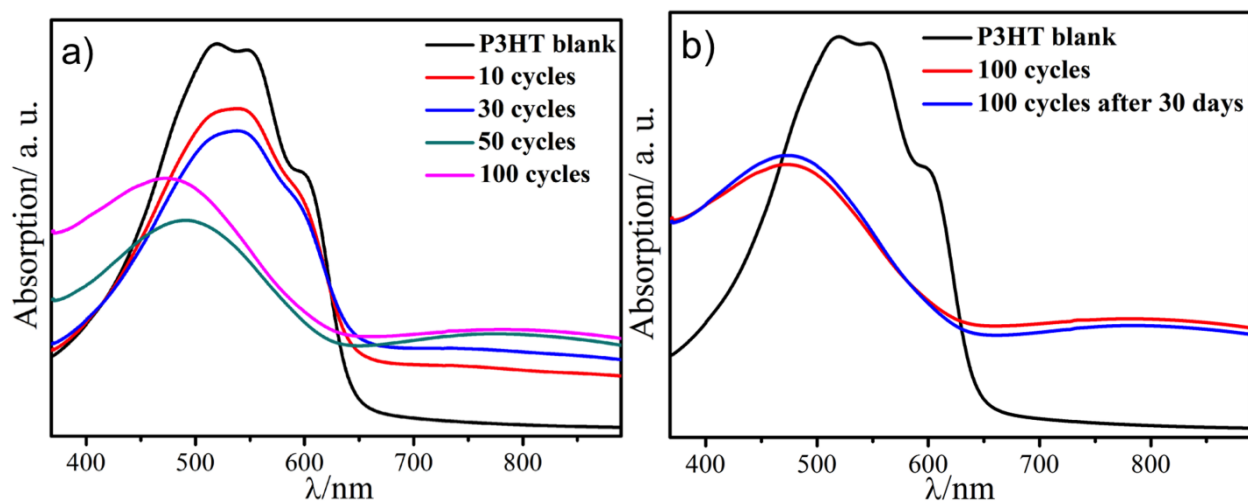


Figure 3, a) UV-Visible absorption spectra showing the 350-890 nm region of untreated P3HT (black) and MoCl_5 -infiltrated P3HT after 10 (red), 30 (blue), 50 (cyan), and 100 (magenta)

infiltration cycles at 70 °C; b) absorption spectra of untreated P3HT (black), MoCl₅-infiltrated P3HT after 100 infiltration cycles as prepared (red), and after 30 days storage at ambient conditions (blue).

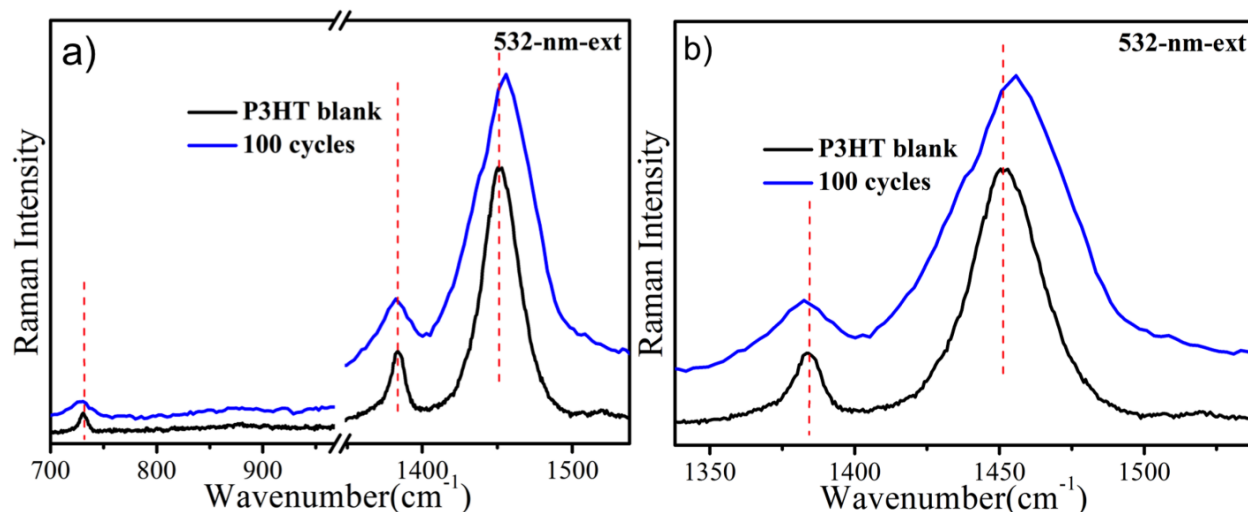


Figure 4, Raman spectra of untreated P3HT, and MoCl₅-infiltrated P3HT after 100 VPI cycles at 70 °C showing a) the 700-1545 cm⁻¹ region, and b) the 1330-1575 cm⁻¹ region.

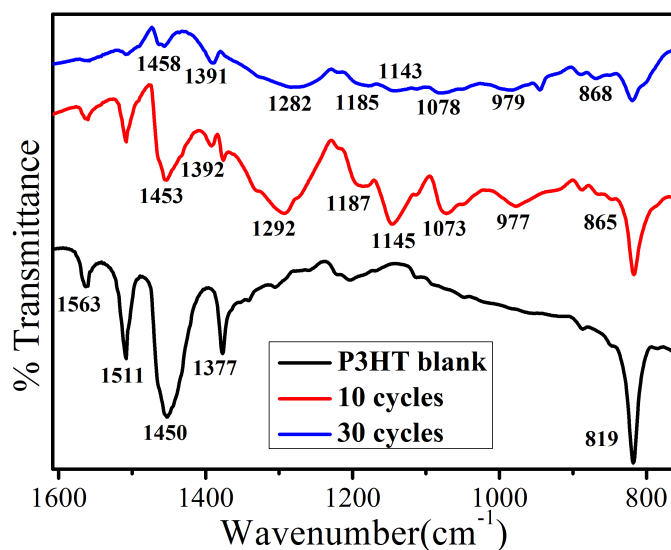


Figure 5, FT-IR spectra (region between 760 and 1610 cm⁻¹) of untreated P3HT (black), and MoCl₅-infiltrated P3HT applying 10 (red) and 30 (blue) infiltration cycles performed at 70 °C.

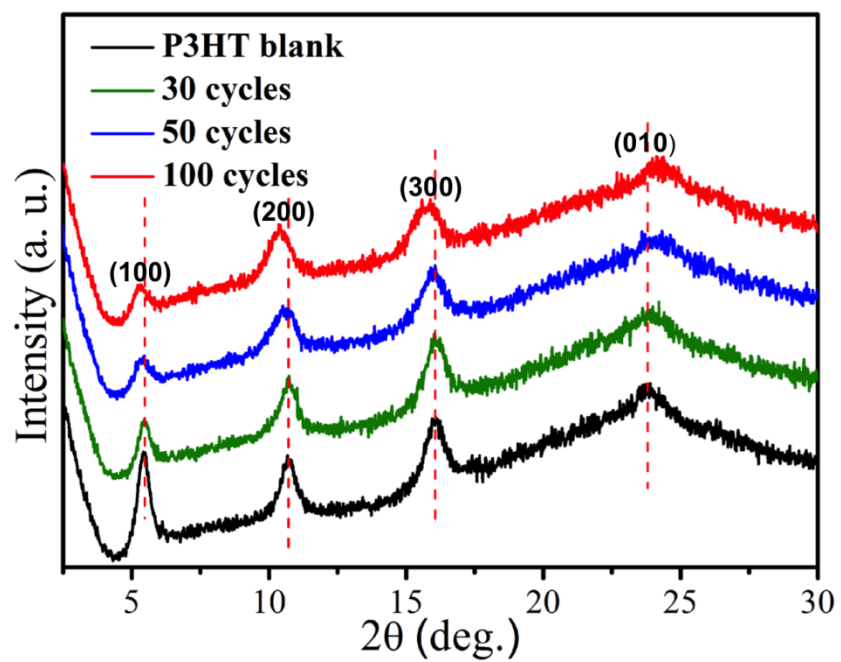


Figure 6, X-ray diffraction spectra of untreated P3HT (black), and MoCl₅-infiltrated P3HT after 30 (green), 50 (blue), and 100 (red) infiltration cycles.

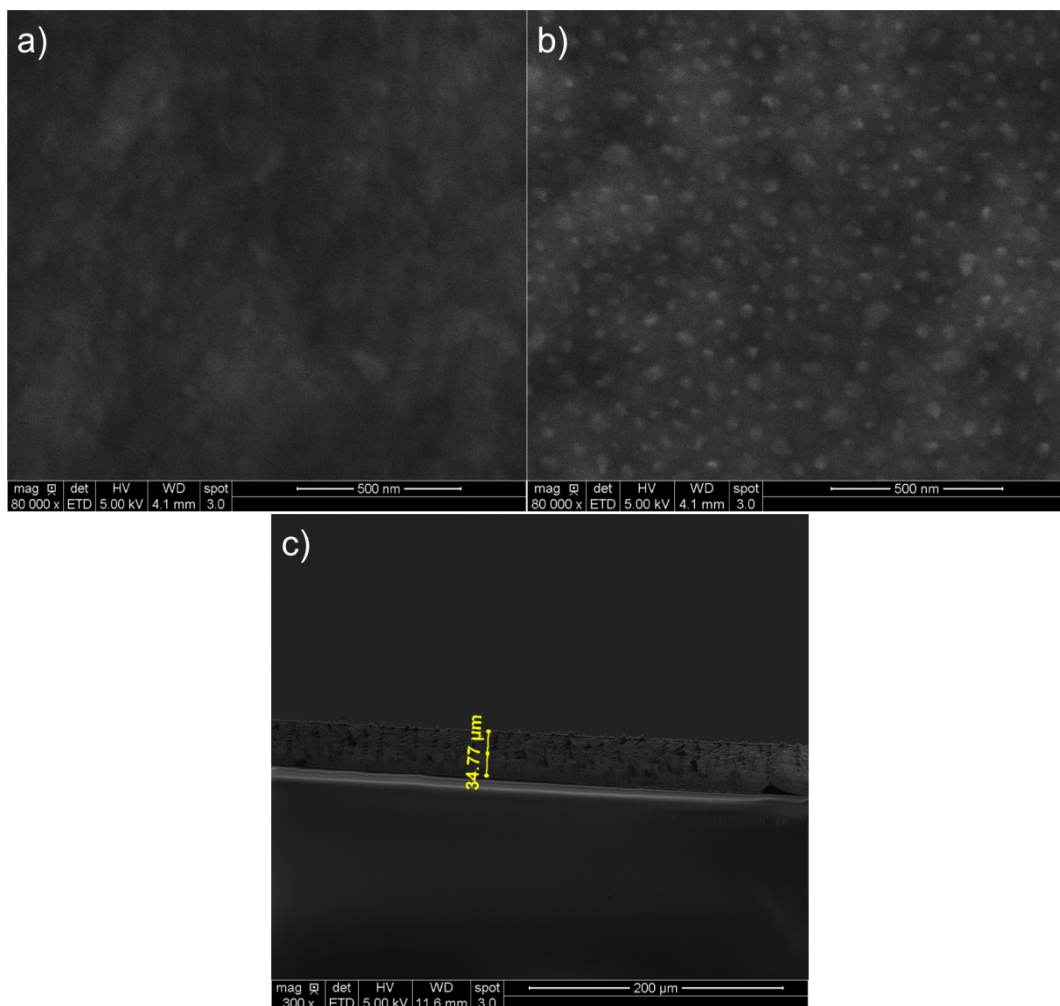


Figure 7, Scanning electron microscopy images of a) untreated P3HT, b) P3HT/MoCl₅ (100 cycles, 70 °C), and c) a low magnification image of the cross-section of the P3HT thin film.

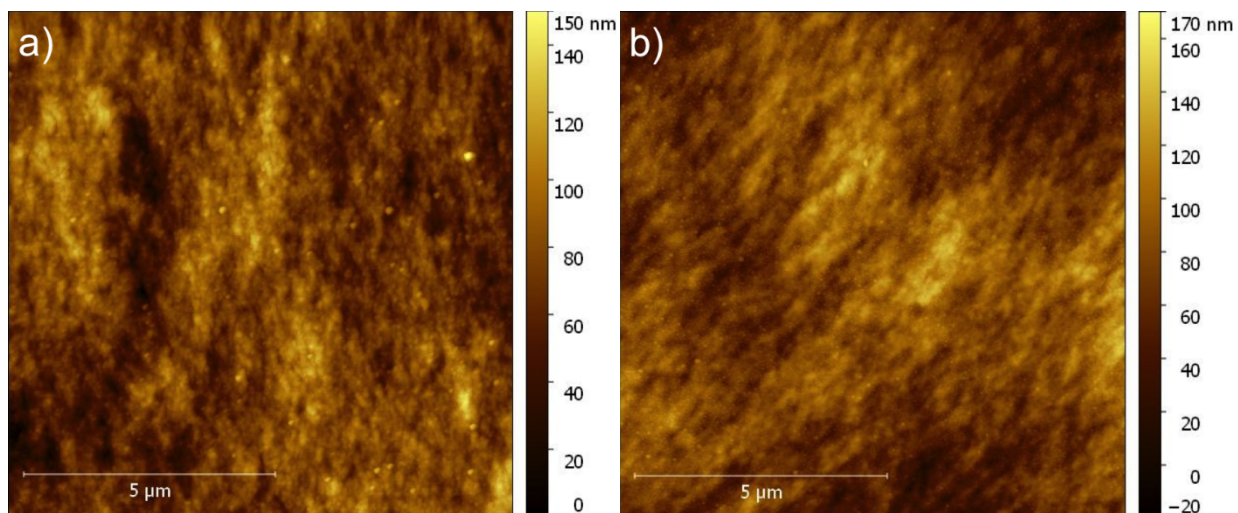


Figure 8, AFM images of a) untreated P3HT, and b) P3HT/MoCl₅ (100 cycles, 70 °C)

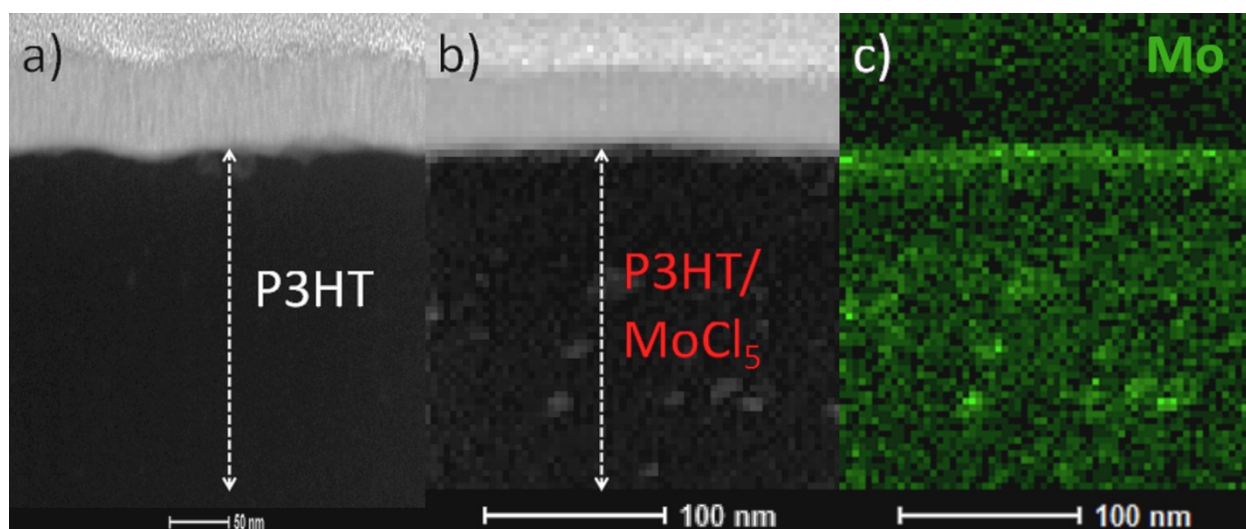


Figure 9, a) TEM image of a cross-sectioned untreated P3HT thin film, b) TEM image of a cross-sectioned MoCl₅-infiltrated P3HT thin film (100 cycles, 70 °C), and c) Mo elemental map of the sample shown in b).

Table 1. Summary of the peak Position and the full width at half maximum (fwhm) of the C=C stretching mode, the C-C stretching mode and the C-S-C deformation mode for untreated P3HT and MoCl₅-infiltrated P3HT after 100 VPI cycles.

Sample	Peak Position and (fwhm) of C=C Mode (cm ⁻¹)	Peak Position and (fwhm) of C-C Mode (cm ⁻¹)	Peak Position and (fwhm) of C-S-C Deformation Mode (cm ⁻¹)
Untreated P3HT	1452 (30)	1384 (11)	731 (9)
P3HT/MoCl ₅ (100cycles)	1457 (47)	1380 (22)	728 (26)

REFERENCES

1. S. R. Forrest, *Nature* **2004**, 428, 911.
2. A. Facchetti, *Chem. Mater.* **2011**, 23,733.
3. H. Sirringhaus, N. Tessler, R. H. Friend, *Science* **1998**, 280, 1741.
4. V. Singh, T. L. Bougher, A. Weathers, Y. Cai, K. Bi, M. T. Pettes, S. A. McMenamin, W. Lv, D. P. Resler, T. R. Gattuso, D. H. Altman, K. H. Sandhage, L. Shi, A. Henry, B. A. Cola, *Nature Nanotech.* **2014**, 9, 384.
5. J. H. Lee, and J. J. Kim, *Physica Status Solidi* **2012**, 209, 1399.
6. M. Pfeiffer, K. Leo, X. Zhou, J. S. Huang, M. Hofmann, A. Werner, and J. Blochwitz-Nimoth, *Organic Electronics* **2003**, 4, 89.

7. M. Gross, D. C. Müller, H. G. Nothofer, U. Scherf, D. Neher, C. Bräuchle, K. Meerhol, *Nature* **2000**, *405*, 661.
8. Y. F. Li, *Acc. Chem. Res.* **2012**, *45*, 723.
9. S. H. Park, A. Roy, S. Beaupre', S. Cho, N. Coates, J. S. Moon, D. Moses, M. Leclerc, K. Lee, A. J. Heeger, *Nature photon.* **2009**, *3*, 297.
10. J. Peet, J. Y. Kim, N. E. Coates, W. L. Ma, D. Moses, A. J. Heeger, G. C. Bazan, *Nature Mater.* **2007**, *6*, 497.
11. Z. C. He, B. Xiao, F. Liu, H. B. Wu, Y. L. Yang, S. Xiao, C. Wang, T. P. Russell, Y. Cao, *Nature photon.* **2015**, *9*, 174.
12. S. Nam, J. Seo, H. Han, H. Kim, S. G. Hahm, M. Ree, Y. S. Gal, T. D. Anthopoulos, D. D. C. Bradley, Y. Kim, *Adv. Mater. Interfaces* **2016**, 1600415.
13. G. Li, R. Zhu, Y. Yang, *Nature photon.* **2012**, *6*, 153.
14. P. Wei, T. Menke, B. D. Naab, K. Leo, M. Riede, Z. N. Bao, *J. Am. Chem. Soc.* **2012**, *134*, 3999.
15. M. F. Calhoun, J. Sanchez, D. Olaya, M. E. Gershenson, V. Podzorov, *Nature Mater.* **2008**, *7*, 84.
16. H. Mendez, G. Heimel, S. Winkler, J. Frisch, A. Opitz, K. Sauer, B. Wegner, M. Oehzelt, C. Rothel, S. Duhm, D. Tobbens, N. Koch, I. Salzmann, *Nat Commun.* **2015**, *6*: 8560.
17. C. H. Gao, X. Z. Zhu, L. Zhang, D. Y. Zhou, Z. K. Wang and L. S. Liao, *Appl. Phys. Lett.* **2013**, *102*, 153301.

18. C. C. Chang, M. T. Hsieh, J. F. Chen, S. W. Hwang, C. H. Chen, *Appl. Phys. Lett.* **2006**, *89*, 253504.
19. D. T. Duong, C. C. Wang, E. Antono, M. F. Toney, A. Salleo, *Organic Electronics* **2013**, *14*, 1330.
20. D. T. Duong, H. Phan, D. Hanifi, P. S. Jo, T. Q. Nguyen, A. Salleo, *Adv. Mater.* **2014**, *26*, 6069.
21. J. Yang, Y. Li, S. Duhm, J. Tang, S. Kera, N. Ueno, *Adv. Mater. Interfaces* **2014**, *1*, 1300128.
22. M. L. Tietze, L. Burtone, M. Riede, B. Lüssem, K. Leo, *Phys. Rev. B* **2012**, *86*, 035320.
23. S. H. Cho, S. W. Pyo, M. C. Suh, *Synthetic Metals* **2012**, *162*, 402.
24. E. F. Aziz, A. Vollmer, S. Eisebitt, W. Eberhardt, P. Pingel, D. Neher, N. Koch, *Adv. Mater.* **2007**, *19*, 3257.
25. P. Pingel, M. Arvind, L. Kölln, R. Steyrlleuthner, F. Kraffert, J. Behrends, S. Janietz, D. Neher, *Adv. Electron. Mater.* **2016**, 1600204.
26. G. C. Welch, G. C. Bazan, *J. Am. Chem. Soc.* **2011**, *133*, 4632.
27. G. C. Welch, R. Coffin, J. Peet, G. C. Bazan, *J. Am. Chem. Soc.* **2009**, *131*, 10802.
28. P. Zalar, Z. B. Henson, G. C. Welch, G. C. Bazan, T. Q. Nguyen, *Angew. Chem., Int. Ed.* **2012**, *51*, 7495.

29. P. Zalar, M. Kuik, Z. B. Henson, C. Woellner, Y. Zhang, A. Sharenko, G. C. Bazan, T. Q. Nguyen, *Adv. Mater.* **2014**, *26*, 724.
30. M. Knez, K. Nielsch, L. Niinistö, *Adv. Mater.* **2007**, *19*, 3425.
31. K. E. Gregorczyk, M. Knez, *Progress in Materials Science* **2016**, *75*, 1.
32. I. Manners, *Science* **2001**, *294*, 1664.
33. C. Sanchez, B. Julián, P. Belleville, M. Popall, *J. Mater. Chem.* **2005**, *5*, 3559.
34. M. J. MacLachlan, M. Ginzburg, N. Coombs, T. W. Coyle, N. P. Raju, J. E. Greendan, G. A. Ozin, I. Manners, *Science* **2000**, *287*, 1460.
35. S. M. Lee, V. Ischenko, E. Pippel, A. Masic, O. Moutanabbir, P. Fratzl, M. Knez. *Adv. Funct. Mater.* **2011**, *21*, 3047.
36. S. M. Lee, E. Pippel, U. Gösele, C. Dresbach, Y. Qin, C. V. Chandran, T. Bräuniger, G. Hause, M. Knez, *Science* **2009**, *324*, 488.
37. S. M. Lee, E. Pippel, O. Moutanabbir, I. Gunkel, T. Thurn-Albrecht, M. Knez, *ACS Appl. Mater. Interfaces* **2010**, *2*, 2436.
38. K. E. Gregorczyk, D. F. Pickup, M. G. Sanz, I. A. Irakulis, C. Rogero, M. Knez. *Chem. Mater.* **2015**, *27*, 181.
39. K. H. Yim, G. L. Whiting, C. E. Murphy, J. J. M. Halls, J. H. Burroughes, R. H. Friend, J. S. Kim, *Adv. Mater.* **2008**, *20*, 3319.

40. J. Cui, D. E. M. Tong, A. Sanz, T. A. Ezquerra, E. Rebollar, A. Nogales, *Macromolecules* **2016**, *49*, 2709.
41. C. Y. Kao, B. Lee, L. S. Wielunski, M. Heeney, I. McCulloch, E. Garfunkel, L. C. Feldman, V. Podzorov, *Adv. Funct. Mater.* **2009**, *19*, 1906.
42. W. C. Tsoi, D. T. James, J. S. Kim, P. G. Nicholson, C. E. Murphy, D. D. C. Bradley, J. Nelson, J. S. Kim, *J. Am. Chem. Soc.* **2011**, *133*, 9834.
43. J. Yamamoto, Y. Furukawa, *J. Phys. Chem. B* **2015**, *119*, 4788.
44. Y. D. Park, J. H. Cho, D. H. Kim, W. H. Lee, K. Cho, *AIP Conf. Proc.* **2007**, *879*, 1623.
45. S. N. Patel, A. M. Glauddell, D. Kiefer, M. L. Chabiny, *ACS Macro Lett.* **2016**, *5*, 268.
46. R. Noriega, J. Rivnay, K. Vandewal, F. P. V. Koch, N. Stingelin, P. Smith, M. F. Toney, A. Salleo, *Nature Mater.* **2013**, *12*, 1038.
47. I. E. Jacobs, E. W. Aasen, J. L. Oliveira, T. N. Fonseca, J. D. Roehling, J. Li, G. Zhang, M. P. Augustine, M. Mascal, A. J. Moulé, *J. Mater. Chem. C*, **2016**, *4*, 3454.

Supplementary Information

Efficient and Controllable Vapor to Solid doping of the Polythiophene P3HT by Low Temperature Vapor Phase Infiltration

Weike Wang,^{a,b,c} Chaoqiu Chen,^a Christopher Tollan,^b Fan Yang,^b Yong Qin^{a*} and Mato Knez^{b,d*}

^aState Key Laboratory of Coal Conversion, Institute of Coal Chemistry, Chinese Academy of Sciences, Taiyuan, 030001, China.

^bCIC nanoGUNE, Tolosa Hiribidea, 76, 20018 Donostia-San Sebastian, Spain.

^cUniversity of Chinese Academy of Sciences, Beijing, 100049, China.

^dIKERBASQUE, Basque Foundation for Science, 48011 Bilbao, Spain.

E-mail: qinyong@sxicc.ac.cn, E-mail: m.knez@nanogune.eu

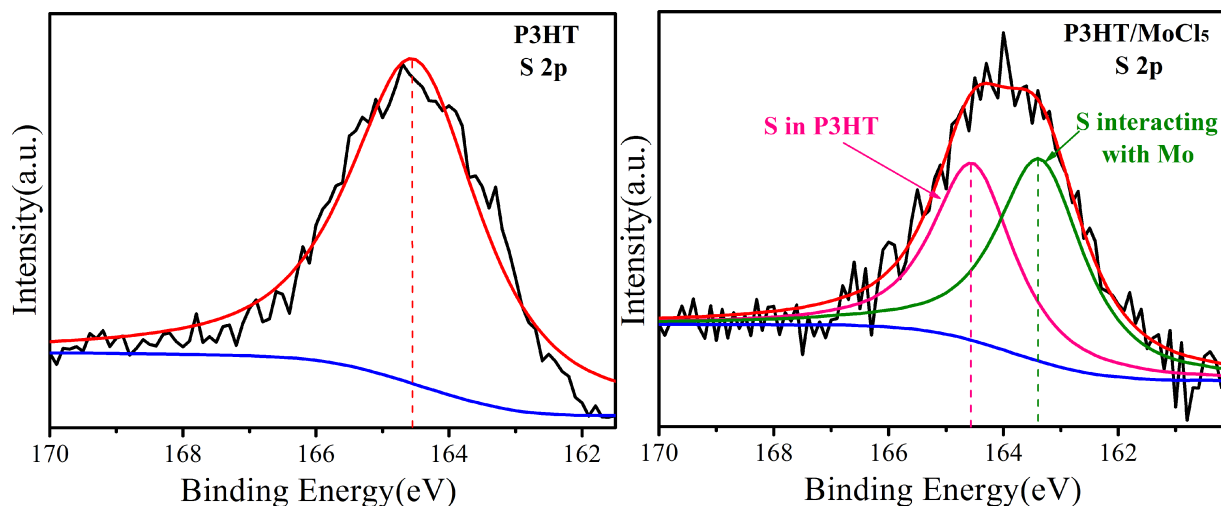


Figure S1. S 2p XPS spectra of pristine P3HT (left), and P3HT/MoCl₅(5 cycles VPI, 70 °C)(right).

In the S 2p XPS spectra, the peak located at binding energy of 164.56 eV corresponds to the S 2p line of the pristine P3HT. While after 5 cycles MoCl₅ infiltration process at 70 °C, the intensity of S 2p line of the pristine P3HT decreases, and a new peak located at binding energy of 163.39 eV developed, which might be due to the S interacting with Mo, indicating the electronic exchange between P3HT and MoCl₅.